REPORT DOCUMENTATION PAGE

Form Approved OMB NO. 0704-0188

1. REPORT DATE (DD-MM-YYYY)	2. REPORT TYPE	3. DATES COVERED (From - To)
04-03-2014	Final Report	1-Oct-2012 - 30-Sep-2013

4. TITLE AND SUBTITLE
Final Report

5a. CONTRACT NUMBER
W911NF-12-1-0600

5b. GRANT NUMBER

5c. PROGRAM ELEMENT NUMBER

6. AUTHORS
Curtis Volin

5d. PROJECT NUMBER

5e. TASK NUMBER

5f. WORK UNIT NUMBER

7. PERFORMING ORGANIZATION NAMES AND ADDRESSES
Georgia Tech Applied Research Corporatior
Office of Sponsored Programs
505 Tenth St., NW
Atlanta, GA 30332 -0001

8. PERFORMING ORGANIZATION REPORT NUMBER

9. SPONSORING/MONITORING AGENCY NAME(S) AND ADDRESS (ES)
U.S. Army Research Office
P.O. Box 12211
Research Triangle Park, NC 27709-2211

10. SPONSOR/MONITOR'S ACRONYM(S)
ARO

11. SPONSOR/MONITOR'S REPORT NUMBER(S)
63115-PH-IRP.1

12. DISTRIBUTION AVAILIBILITY STATEMENT
Approved for Public Release; Distribution Unlimited

13. SUPPLEMENTARY NOTES
The views, opinions and/or findings contained in this report are those of the author(s) and should not contrued as an official Department of the Army position, policy or decision, unless so designated by other documentation.

14. ABSTRACT
Future progress in trapped-ion quantum information processing (QIP) depends on the miniaturization and integration of ion trapping technologies. With large-scale microfabrication of trapping structures now well advanced, the trapped-ion QIP community has recently turned to the task of integrating light collection optics with traps in a scalable fashion. We consider scalability to be defined by the ability to add additional lenses to collect light from additional ions without reducing performance or substantially increasing complexity (e.g., reduced collection efficiency and increased optomechanical alignment requirements, respectively). We report here on the

15. SUBJECT TERMS
Integrated optics, ion traps

16. SECURITY CLASSIFICATION OF:			17. LIMITATION OF ABSTRACT	15. NUMBER OF PAGES	19a. NAME OF RESPONSIBLE PERSON
a. REPORT	b. ABSTRACT	c. THIS PAGE			Curtis Volin
UU	UU	UU	UU		19b. TELEPHONE NUMBER 404-407-8487

Report Title

Final Report

ABSTRACT

Future progress in trapped-ion quantum information processing (QIP) depends on the miniaturization and integration of ion trapping technologies. With large-scale microfabrication of trapping structures now well advanced, the trapped-ion QIP community has recently turned to the task of integrating light collection optics with traps in a scalable fashion. We consider scalability to be defined by the ability to add additional lenses to collect light from additional ions without reducing performance or substantially increasing complexity (e.g., reduced collection efficiency and increased optomechanical alignment requirements, respectively). We report here on the development and preliminary testing of the first collection optic integrated with a microfabricated ion trap that satisfies these criteria for scalability. We demonstrate that these integrated optics are readily fabricated using standard processes, are robust to normal bakeout procedures for ion traps (200C), and are capable of collecting ion fluorescence comparable to state-of-the-art non-scalable objective systems. With dozens of trap die completed and three packaged and tested, we expect testing and application of these optics to continue well beyond the completion of the IDM program.

Enter List of papers submitted or published that acknowledge ARO support from the start of the project to the date of this printing. List the papers, including journal references, in the following categories:

(a) Papers published in peer-reviewed journals (N/A for none)

Received Paper

TOTAL:

Number of Papers published in peer-reviewed journals:

(b) Papers published in non-peer-reviewed journals (N/A for none)

Received Paper

TOTAL:

Number of Papers published in non peer-reviewed journals:

(c) Presentations

Number of Presentations: 0.00

Non Peer-Reviewed Conference Proceeding publications (other than abstracts):

Received Paper

TOTAL:

Number of Non Peer-Reviewed Conference Proceeding publications (other than abstracts):

Peer-Reviewed Conference Proceeding publications (other than abstracts):

Received Paper

TOTAL:

Number of Peer-Reviewed Conference Proceeding publications (other than abstracts):

(d) Manuscripts

Received Paper

TOTAL:

Number of Manuscripts:

Books

Received Paper

TOTAL:

Patents Submitted

Patents Awarded

Awards

Graduate Students

NAME	PERCENT_SUPPORTED

FTE Equivalent:
Total Number:

Names of Post Doctorates

NAME	PERCENT_SUPPORTED

FTE Equivalent:
Total Number:

Names of Faculty Supported

NAME	PERCENT_SUPPORTED

FTE Equivalent:
Total Number:

Names of Under Graduate students supported

NAME	PERCENT_SUPPORTED

FTE Equivalent:
Total Number:

Student Metrics

This section only applies to graduating undergraduates supported by this agreement in this reporting period

The number of undergraduates funded by this agreement who graduated during this period: 0.00

The number of undergraduates funded by this agreement who graduated during this period with a degree in science, mathematics, engineering, or technology fields:..... 0.00

The number of undergraduates funded by your agreement who graduated during this period and will continue to pursue a graduate or Ph.D. degree in science, mathematics, engineering, or technology fields:..... 0.00

Number of graduating undergraduates who achieved a 3.5 GPA to 4.0 (4.0 max scale):..... 0.00

Number of graduating undergraduates funded by a DoD funded Center of Excellence grant for Education, Research and Engineering:..... 0.00

The number of undergraduates funded by your agreement who graduated during this period and intend to work for the Department of Defense 0.00

The number of undergraduates funded by your agreement who graduated during this period and will receive scholarships or fellowships for further studies in science, mathematics, engineering or technology fields:..... 0.00

Names of Personnel receiving masters degrees

NAME

Total Number:

Names of personnel receiving PHDs

NAME

Total Number:

Names of other research staff

NAME PERCENT_SUPPORTED

FTE Equivalent:
Total Number:

Sub Contractors (DD882)

Inventions (DD882)

Scientific Progress

See attached.

Technology Transfer

IDM Final Report

December 31, 2013

Georgia Tech Research Institute

Griffith University

Abstract

Future progress in trapped-ion quantum information processing (QIP) depends on the miniaturization and integration of ion trapping technologies. With large-scale microfabrication of trapping structures now well advanced, the trapped-ion QIP community has recently turned to the task of integrating light collection optics with traps in a scalable fashion. We consider scalability to be defined by the ability to add additional lenses to collect light from additional ions without reducing performance or substantially increasing complexity (e.g., reduced collection efficiency and increased optomechanical alignment requirements, respectively). We report here on the development and preliminary testing of the first collection optic integrated with a microfabricated ion trap that satisfies these criteria for scalability. We demonstrate that these integrated optics are readily fabricated using standard processes, are robust to normal bakeout procedures for ion traps (200C), and are capable of collecting ion fluorescence comparable to state-of-the-art non-scalable objective systems. With dozens of trap die completed and three packaged and tested, we expect testing and application of these optics to continue well beyond the completion of the IDM program.

Table of Contents

1 Introduction

1.1 *Overview*

The efficient collection of fluorescence emission from trapped ions impacts quantum computing and communication applications by enabling a substantial speedup in ion-to-photon and remote ion-to-ion quantum entanglement rates and by decreasing the time required to read out the ion states. Particularly in the case of quantum information technology, reduction of the size of the collection optic to size scales consistent with expected trap densities (10s to 100s of microns between ions) represents a significant step towards demonstration of a scalable optical architecture.

For the Integrated Diffractive Mirrors (IDM) seedling, the Quantum Information Systems group at the Georgia Tech Research Institute (GTRI) and the Kielpinski group at Griffith University have teamed to demonstrate a diffractive mirror integrated into the surface of a microfabricated ion trap. Because these diffractive mirrors are contained entirely within the existing electrode structure, they neither alter the electromagnetic environment seen by the ion nor do they restrict optical or electrical access. The result is a substantial increase the density of optical interconnects on the ion trap beyond any integrated system demonstrated to date.

Finally, the lithographic microfabrication of these optics into the trap eliminates optomechanical alignment requirements, especially thermomechanical movement and stress during bakeout and/or cooling to cryogenic temperatures.

We demonstrate loading of IDM traps with four-level optics at both GTRI and Griffiths. Each trap contains five, four-level collimation optics designed to demonstrate high efficiency fluorescence collection (NA = 0.63). The inferred multimode collection efficiency of the collimation optics is 2.5-4.0%, with those values expected to improve when measured. Taking advantage of the unprecedented optical interconnect density, each trap also contains three, four-level test optics for exploring future potential applications. Shuttling over the self-imager test optic shows the lateral alignment of the mirror to be within 1 μm of the trap axis. This is consistent with the design tolerance of the collimation optics for single-mode collection. We have acquired images of single ions through the diffractive mirror.

1.2 *Background*

1.2.1 Scalable fluorescence collection

Future progress in trapped-ion quantum information processing (QIP) depends on the miniaturization and integration of ion trapping technologies. With large-scale microfabrication of trapping structures now well advanced, the trapped-ion QIP community has recently turned to the task of integrating light collection optics with traps in a scalable fashion. There are two distinct sets of requirements on collection optics, depending on the QIP application of interest:

1. Multimode light collection, suitable for ion state detection. The figure of merit is the collection efficiency η_0 , i.e. the fraction of ion fluorescence collected onto a single-pixel light

detector (normally a photomultiplier tube). Alternately, the light may be coupled to a detector through a multimode fiber. The resolution of the optic is constrained only to the ability to resolve simultaneous measurements on multiple ions.

2. Single-mode collection, suitable for both state detection and quantum communication. In addition to high collection efficiency, the collection optic must achieve near-diffraction-limited performance, as characterized by, e.g., mode matching into a single-mode fiber. An appropriate figure of merit is $\eta_{SM} = \eta_0 / M^2$, where M^2 is the standard quality parameter defined for Gaussian beams. η_{SM} gives the fraction of ion fluorescence collected into a single-mode fiber.

1.2.2 Fresnel and diffractive mirrors

The diffractive mirror proposed here is the only scalable technology that can be integrated into current trapped-ion QIP architectures for both multimode and single-mode light collection (Fig. 1). A Fresnel mirror is an analytic diffractive optic that approximates the shape of a bulk curved mirror so that an optical wave incident on the Fresnel mirror receives a position-dependent phase shift equal to that given by the equivalent bulk mirror. The relationship between a Fresnel mirror and a bulk mirror is analogous to that between a Fresnel lens and a bulk lens, except that the former works by reflection and the latter by refraction. Like Fresnel lenses, Fresnel mirrors can be fabricated by approximating the ideal surface curvature by a stepped profile of two or more levels, removing 2π optical phase steps at appropriate intervals so as to maintain a near-planar structure. For the typical azimuthally symmetric profile, the Fresnel mirror is then specified by the step spacings and heights.

Fresnel mirrors of high solid angle coverage (up to 0.5 NA) and diffraction efficiency are easier to design than Fresnel lenses of the same specifications. Fresnel lenses are subject to interference effects that lower diffraction efficiency at moderate angles. Fresnel mirrors are predicted to be free from these effects, however, a reduction in phase contrast for the step profile at high angles of incidence (NA>0.5) substantially reduces the collection efficiency for high numerical aperture. Generalizing the profile of the diffractive reflective optic using a suitable optimization technique (e.g., genetic optimization) maintains constant diffraction efficiency above 95% even at solid angle coverage near 50% [1]. The reflectivity of aluminum over the UV spectrum of interest for ion trapping is 92% and this factor sets the primary limit to collection efficiency. The upper limit to collection efficiency is therefore 44%. Microfabricated diffractive mirrors with 6% solid angle coverage and 77% diffraction efficiency were reported in the 1990's [2]. Increasing the solid angle to near 50% is simply a matter of reducing feature size to the scale already reported in transmissive Fresnel lenses [**Error! Bookmark not defined.**].

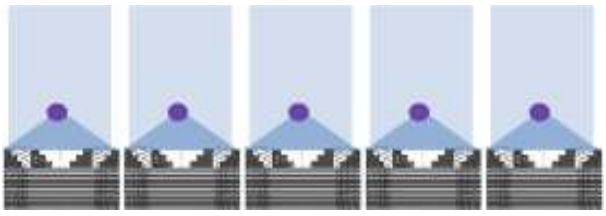

Figure 1. Integration of diffractive mirrors into surface ion traps. The mirror surface also acts as trap electrodes. Fluorescence from trapped ions is collected at high solid angle coverage for subsequent coupling into optical fiber (not shown).

2 Fabrication

2.1 *Layout*

We adopted a conservative design approach for the Integrated Diffractive Mirrors (IDM) trap, in keeping with the project proposal. The electrode layout of the IDM trap is identical to the existing Microwave I (MI) design.[3] The only design difference between the IDM and MI traps was the addition of the diffractive optics, which were confined to the central ground electrode. Figure 2 shows a schematic of the IDM trap, including both trap electrodes and diffractive optics.

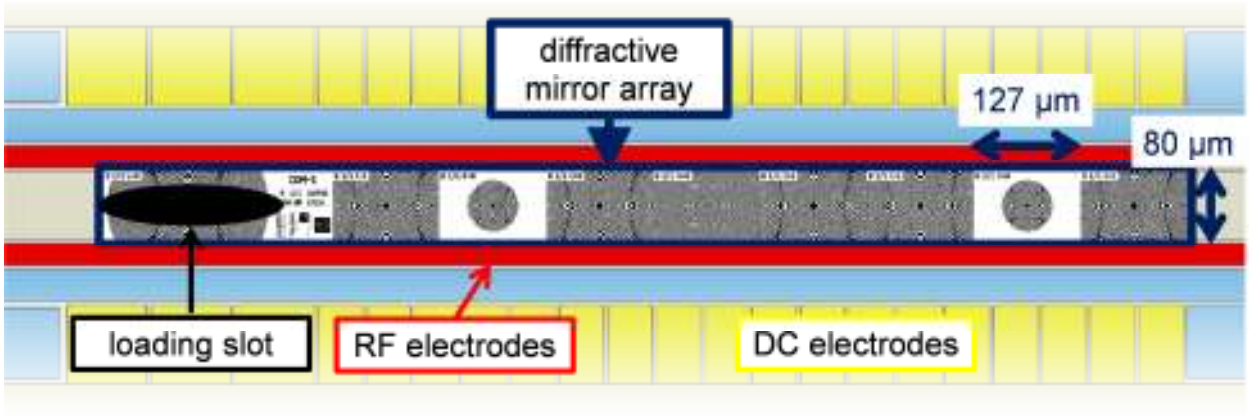

Figure 2. Top-level design schematic of the Integrated Diffractive Mirrors (IDM) trap. The electrode structure is identical to that of the Microwave I trap. An array of diffractive mirrors is printed on the ground electrode.

The diffractive optic array consists of the main array (right 8 optics in Figure 2 and Figure 3), a collimating mirror on the loading region (far left in Figure 2), separated by a labeling/logo region. The pitch of the main array along the trap axis was chosen at 127 µm for compatibility with commercial integrated optics and fiber ribbon. The width of all optics was set by the ground electrode width of 80 µm. Since the trapping potential minimum was nominally 58.6 µm above the trap surface, the numerical aperture of each element in the main array is 0.63, similar to that of the Fresnel lens used in the Griffith team's previous experiments [Streed11, Jechow11].

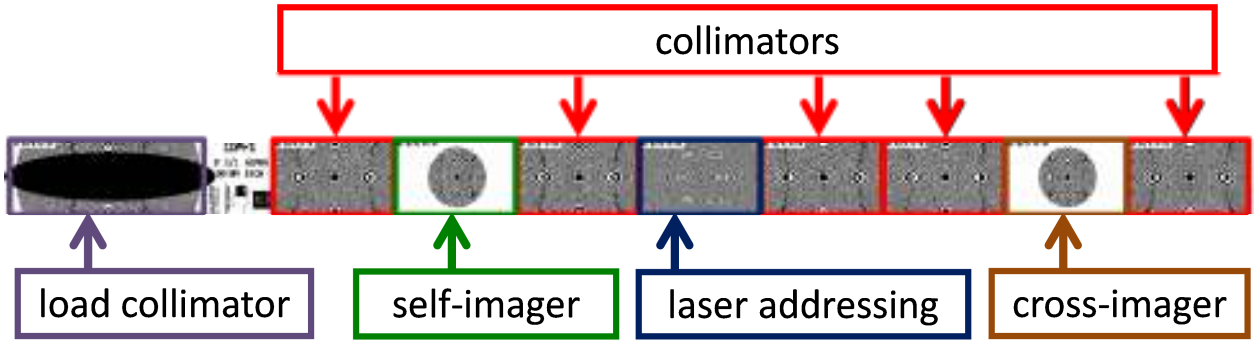

Figure 3. Schematic of the diffractive optics array.

The main optics array consists of 5 collimating mirrors and three test optics for exploring future potential applications of diffractive mirrors in ion QIP (Figure 3). Each collimating mirror was designed to collimate isotropic radiation at 369.5 nm originating from a point at the nominal ion height. The test optics include (1) a "self-imager," designed to refocus ion fluorescence back onto the ion itself, (2) a "laser addressing" optic, designed to focus a collimated laser beam onto an ion above the neighboring collimation optic, and (3) a "cross-imager", designed to image an ion onto a neighboring ion 20 um away.

The loading zone collimator is 200 μm long, but most of its surface area is actually ablated away during fabrication of the loading slot. Hence its numerical aperture is not well known. However, we believed it was worthwhile to include this optic so that we could immediately proceed to imaging without the need for shuttling the ions. In fact, time constraints prevented Griffith from performing ion shuttling, but we obtained significant data from the loading zone collimator.

2.2 *Design of diffractive optical structures*

The Griffith team performed all optical design in this project, from initial conception to the provision of final mask designs for wafer-level lithographic definition of the diffractive optics. The design flow comprised the following steps: (1) ray-tracing design, (2) grating structure design, (3) single-optic mask generation, (4) array-level mask generation, (5) wafer layout.

For each type of optic in the array, we implemented a realistic ray-tracing model in ZEMAX. The ray-tracing model was used to derive an optical phase function for the optic that minimized aberrations. We also evaluated the effect of fabrication errors on the optical aberrations. All designs were essentially aberration-free for the expected fabrication tolerance of 1 μm. Errors in the ion height were found to be the dominant source of aberration.

Next, we designed 2-level and 4-level grating structures to implement these phase functions. Diffraction efficiencies were calculated using two independent rigorous coupled-wave vector diffraction solvers, GSolver and GD-Calc. Genetic optimization was used to define an ideal grating profile and find its diffraction efficiency. The lithographic fabrication constraints were then added by hand and the designs were tweaked to approximate the optimum diffraction efficiency. As shown in Figure 4, the final 4-level design used equal step widths and heights, with each step being 45 nm high. This design yielded 60 – 80% diffraction efficiency and low polarization-dependent loss over most of the required range of grating periods. The final 2-level design also used equal step widths and heights, but with a 90 nm step height. This design yielded 30 – 40 % diffraction efficiency.

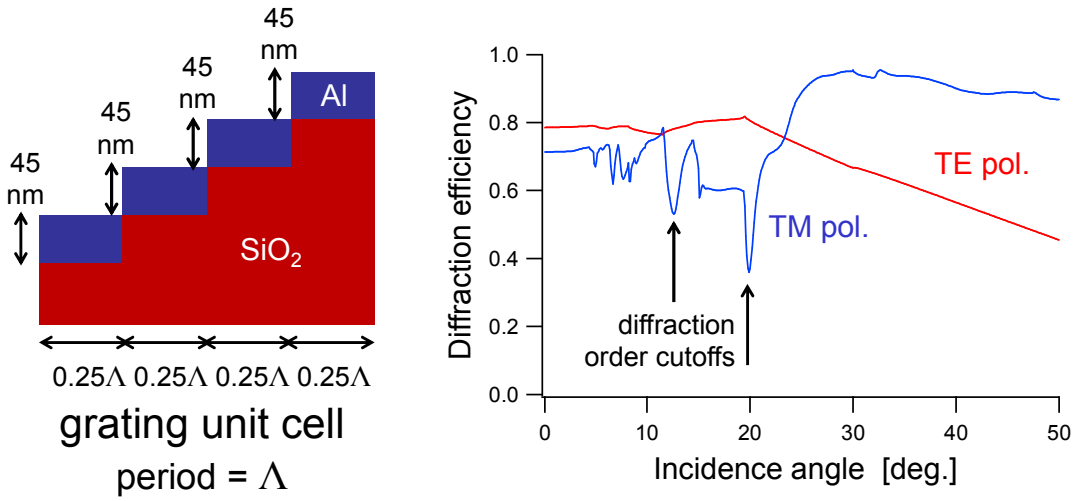

Figure 4. Left: Final design for the 4-level grating structures. Right: Simulated diffraction efficiency as a function of the incidence angle of light.

To generate masks for individual optics, we approximated the ideal phase function from the ray-tracing design using a stepped phase profile. Three types of masks were generated: the so-called four-level (F), hybrid (H), and binary (B) masks. These masks were adapted to provide different levels of tolerance to fabrication error. The F and B masks used the 4-level and 2-level designs everywhere, while the H masks used the 4-level design for feature sizes greater than 200 nm and the 2-level design for smaller features. In every case, the parts of the masks with feature size less than 100 nm were removed. The masks were generated as PNG format graphics with typical size 250 kB.

In assembling the single-optic masks into masks for the whole array, we attempted to defend against an unknown systematic offset of the ion height. Although the ion height is precisely known by simulation, the accuracy of the simulation has never been experimentally confirmed to the required level (the optical aberrations become significant if the ion height is offset by 2 μm). Pushing the ion to the correct height with electric fields is not an acceptable solution since excessive micromotion would be incurred. A wide variety of masks for different ion heights was therefore designed for each optic, according to the procedures above. Four different array-level masks, labeled α, β, γ, and δ, were assembled from the single-optic masks, using different combinations of ion height offsets for the individual optics. By this means, we aimed to obtain at least a few chips whose optics would match the actual ion heights, as determined by subsequent testing.

Finally, in assembling the array-level masks into a wafer-level design, we attempted to defend against a possible lateral offset between the lithography defining the optical array and the lithography defining the trap electrodes. Our estimate for the maximum lateral offset error was 1 μm, within the acceptable tolerance for aberration-free optical performance. However, we felt that a conservative approach to this issue was appropriate: as for the ion height, it would not be acceptable to push the ion transversely to the trap axis owing to micromotion (although axial pushing would be acceptable since this does not incur micromotion). The wafer-level design incorporated deliberate offsets of the array-level optics designs relative to the nominal

electrode positions. Again, by inspection of the completed IDM wafers, we aimed to select chips with small lateral offset error. The entire wafer layout, incorporating the height-variant arrays and their lateral offsets, is shown in Figure 5. Each wafer used either the F designs, the H designs, or the B designs – in no case were these designs combined on a single wafer.

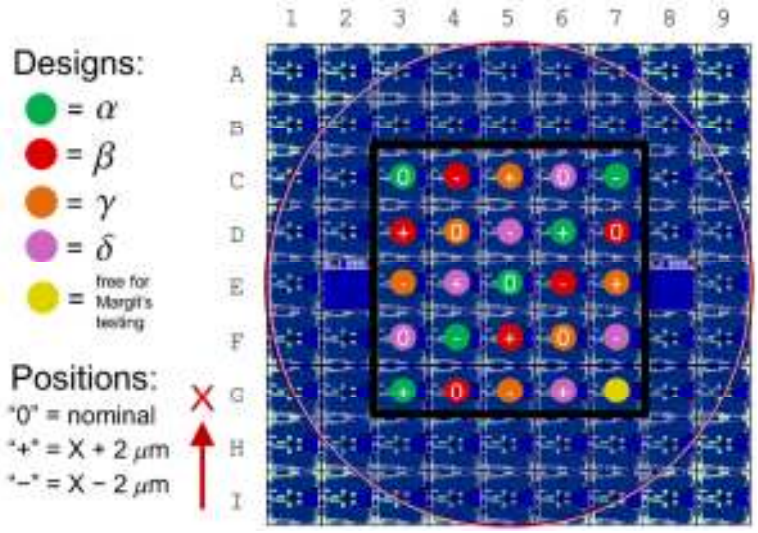

Figure 5. Complete layout of a single wafer, incorporating defense against both ion height errors and lateral offset errors.

2.3 *Fabrication*

Fabrication of ion trap devices with integrated diffractive optical elements (DOE) was undertaken at GTRI in conjunction with the Fraunhofer Heinrich-Hertz Institute (FHHI). The main fabrication task in this project began with creating a process flow that worked with the existing ion trap fabrication process developed at GTRI as well as the requirements of FHHI and their electron beam lithography system. In order to successfully create devices it was essential to share our capabilities, design requirements, and material sets with FHHI and learn about the material characteristics they needed to create a high quality DOE. The requirements from FHHI included alignment marks etched 1.5-2 μm deep with reproducible dimensions and vertical sidewalls, a very smooth oxide surface (<5nm RMS roughness), and uniform oxide thickness across the wafer. The challenge for GTRI was developing a process flow that met these requirements and allowed the ion trap fabrication to be completed without destroying the DOE features.

With these challenges in mind we decided to create the DOE in our devices after our standard 10 μm oxide deposition. At this point in the process the surface is a uniform thickness oxide with surface roughness on the order of 10-20 nm. A chemical mechanical polishing (CMP) step for the oxide surface was added to the standard process flow to reduce surface roughness below the 5 nm RMS required by FHHI for their electron beam lithography process. GTRI also developed an oxide etch recipe with a photoresist mask that produced the 1.5-2 μm depth and vertical sidewalls required by FHHI. These processes were tested and sample wafers sent to FHHI to confirm suitability before device wafers were fabricated. Upon developing these

processes GTRI was able to send samples with the cross section presented in Figure 6 to FHHI for final DOE fabrication.

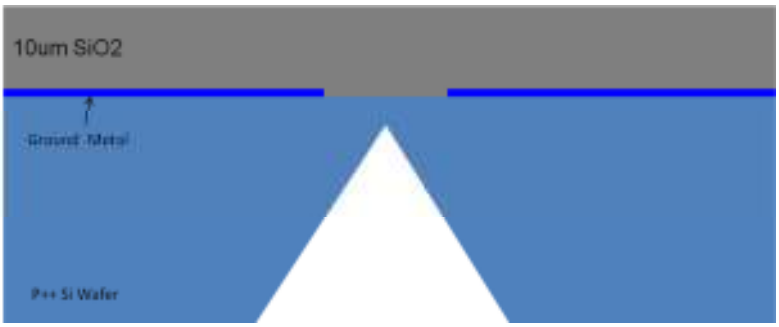

Figure 6: Device cross section following CMP as delivered to FHHI for DOE fabrication

Upon receipt of these samples FHHI created two- and four-level DOE structures using electron beam lithography, leaving the DOE patterned in the oxide surface (Figure 7, DOE not to scale). These samples were shipped back to GTRI for completion of the ion trap fabrication process. In order to maximize the chances of project success FHHI fabricated three different DOE designs: binary, four-level, and hybrid. The binary design has only two height levels in the DOE, four-level has four height levels, and hybrid has four levels on the big features and only two levels on the smaller features. During fabrication, FHHI decided that the four level structures could not be made reliably due to the overly aggressive feature sizes and alignment tolerances required. Binary and hybrid designs were fabricated successfully by FHHI and delivered to GTRI for further processing. The etch depth measured by FHHI using the AFM was 45-50nm per step, within 5% of the nominal value. Figure 8 shows representative samples of the binary and hybrid devices delivered by FHHI to GTRI.

Figure 7 Cross section as delivered by FHHI after DOE fabrication (DOE not to scale)

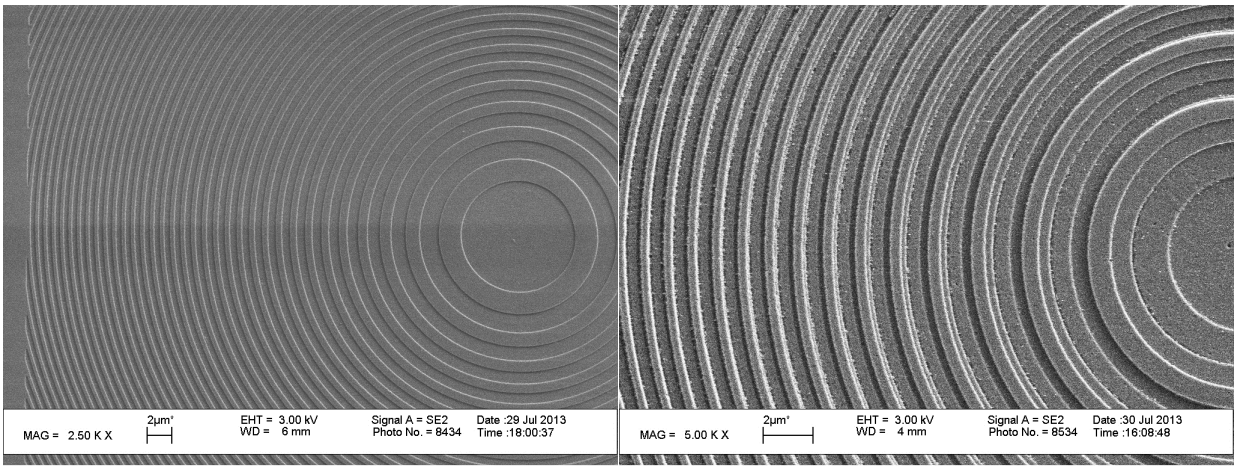

Figure 8: Binary (left) and Hybrid (right) DOE's as received from FHHI.

At this point in the project the important factors considered when designing the process included:

- Coating the DOE with metal without washing out or destroying the features
- Electrically connecting this metal with our center ground electrode
- Protecting the DOE during the subsequent processing of the DC/RF electrode metal and top ground
- Keeping the DOE surface at the same height as the subsequent thick RF/DC metal layer
- Cleanly removing any protection once the processing was complete in order to reveal the DOE

After a series of tests on a sample device measuring metal conductivity as well as feature resolution, a metal thickness of 100 nm aluminum on the DOE was determined to be ideal. In final device processing this thickness of metal did change the feature dimensions slightly (increasing ridge width and decreasing trench width) but the features were slightly overdeveloped originally (making the ridges thinner and the trenches wider than design) so the dimension change brought them back to the design specification (Figure 9).

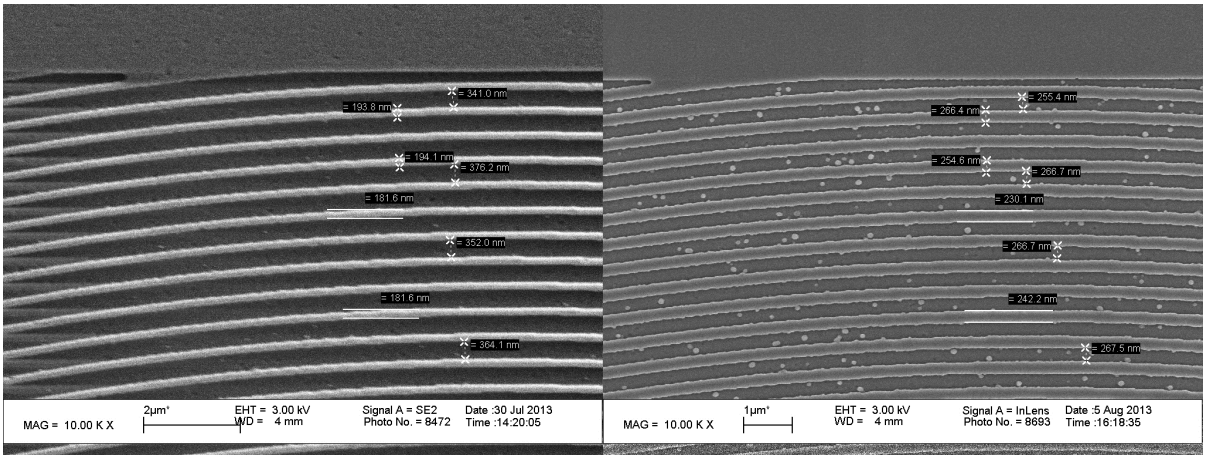

Figure 9: Small DOE features as received and after metal deposition

Once deposited, the DOE metal is patterned and plasma etched in an inductively coupled plasma (ICP) tool. Otside of the optics, the etch process is continued into the oxide (overetch) so the final DOE metal surface will be at the same height as the DC/RF metal layer (Figure 10, shown before addition of the DC/RF metal layers). After the DOE metal is patterned, a 1 um thick oxide layer is deposited to protect the DOE structure during subsequent processing (Figure 11). Openings are created in the oxide protection layer away from the DOE features for electrical connection to the center ground electrode.

Figure 10: Completion of DOE Metal Etch.

Figure 11: DOE Protection Oxide

A 1 μm thick metal layer is deposited and patterned to create RF and DC electrodes with the oxide layer over the DOE protecting it from the effects of the ICP aluminum etch (Figure 12). Following metal deposition 1 μm of oxide is deposited to electrically insulate the DC electrodes from the top ground layer. The final deposition is a 1 um thick metal layer that is patterned to create the top ground and large top DC electrodes (Figure 13). Once the final metal layer is patterned the DOE is further protected with a 10 um thick photoresist while oxide is etched in the loading slot and the gaps between electrodes. The backside loading slot is then opened and finally the DOE protection oxide is removed revealing the final DOE surface and completing the fabrication process (Figure 14).

Figure 12: DC/RF Metal Deposition and Etch

Figure 13: Top metal pattern and etch

Figure 14: Final Device Cross Section

A number of working ion trap die of both the binary and hybrid diffractive optical element design were successfully fabricated with this process. The following images show the binary and hybrid DOE elements after successful ion trap fabrication (Figure 15). Additional images include an SEM of one full DOE element (Figure 16), an optical microscope image of the ion trapping zone with nine diffractive optical elements along the length of the trap (Figure 17), and a dark-field microscope image of a number of DOE's in a finished trap (Figure 18).

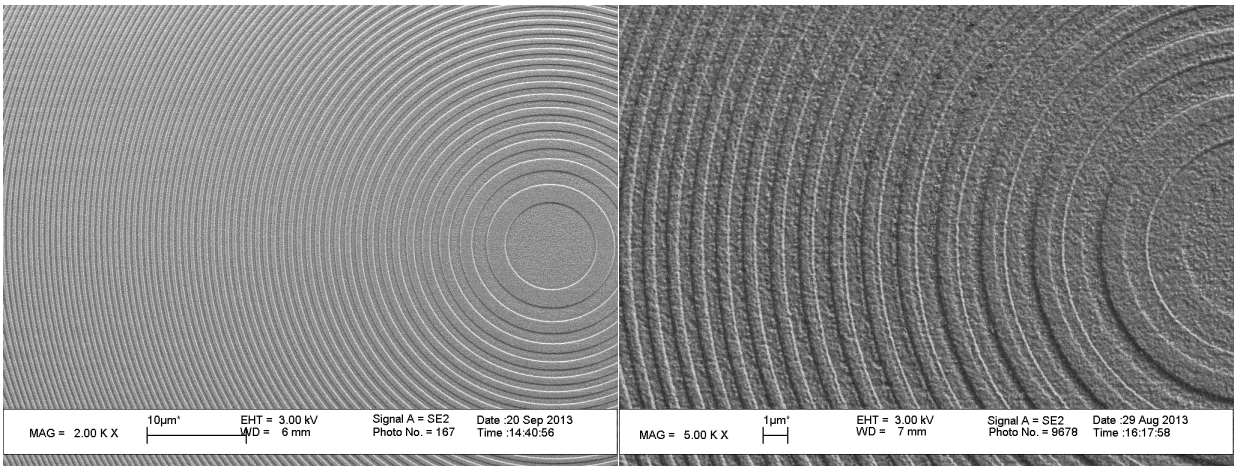

Figure 15: Binary (left) and Hybrid (right) DOE after completed ion trap fabrication

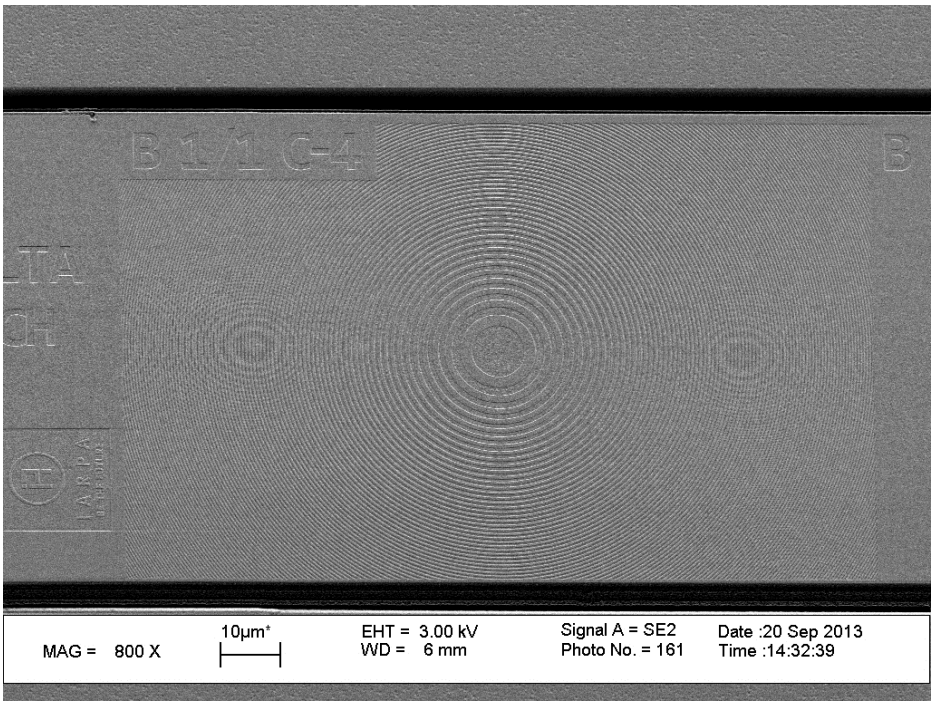

Figure 16: Full Binary DOE on a completed ion trap

Figure 17: Optical microscope image of active ion trapping zone with nine diffractive optical elements

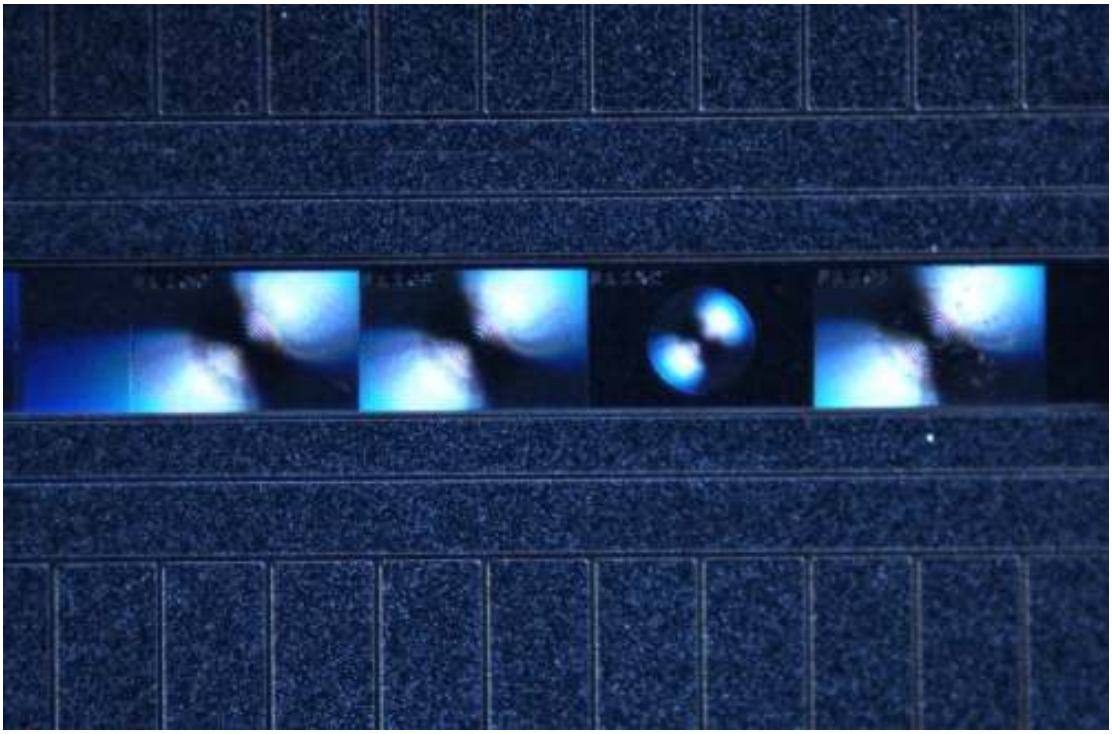

Figure 18: Dark field image of DOE's on completed ion trap

2.4 *Alternate fabrication techniques*

We researched nanoimprinting as an attractive alternate technique for fabrication of optics in future programs. The science of nanoimprinting into metal films is in its infancy, but such techniques offer great promise for overcoming multilevel- and trap-misalignment issues and feature size limitations imposed by conventional lithography fabrication. The pressures typically required to imprint in metal films are on the order of 1 GPa,[4] which is on the order of the fracture stress for Silicon wafers.[5] The transfer of precise patterns required to achieve high diffraction efficiency would require a great deal of study and optimization. While we have identified academic experts in nanoimprint technology with potential collaborative interest, development of this technology is consigned to a future program.

3 Trapping hardware

3.1 *GTRI testing station*

The design and operation of GTRI's microwave ion trap and testing stations are described elsewhere.[3,6,7] The principal difference from prior documented testing is the use of an 0.28 NA Ealing Optics reflective objective (X15/0.28, currently sold by Edmund Optics, 66-576). All experiments performed at GTRI used Calcium ions (λ = 397nm).

3.2 *Griffith testing station*

3.2.1 Vacuum system

We constructed a new vacuum system for operating the microfabricated traps which was similar, but not identical to, those used at GTRI. Our system, centered on a Kimball Physics MCF600-SO200800 "spherical octagon" chamber, was intended to afford more optical access and improved vacuum conductance.

A 1 m x 1.5 m walk-in clean room (specified at class 10,000) was constructed at Griffith for handling of microfabricated traps and associated hardware. The trap vacuum chamber for the microfabricated trap was assembled in the clean room. A trap socket and associated hardware were installed substantially as at GTRI. In particular, the trap socket was assembled at GTRI using parts machined at Griffith.

After assembly, we attempted to follow the GTRI baking procedure, in which a new socket is initially baked at 250 C for approximately 2 weeks. During this time the chamber was pumped by a turbopumping system with a base pressure of 10^{-8} torr. The conductance-limited pumping speed at the chamber was estimated at 10 L/s. Since we lack an industrial oven, we used heater tapes and aluminum foil to construct a temporary oven, as done in many labs. We controlled the temperature using manual Variacs to drive the heater tapes, while taking regular thermocouple readings at many points on the chamber to ensure even heating to the desired level.

Outgassing data was acquired throughout the bakeout using a residual gas analyser (RGA). We observed high partial pressures of phenol, benzene, and hydrocarbon fragments. These data are indicative of PEEK outgassing, since PEEK is essentially a phenolic polymer. The bake was terminated when the trap chamber contribution to RGA readings became negligible. The ion pump, ion gauge, and titanium sublimation pump were thoroughly degassed before cooling down the chamber.

This baking procedure radically failed. After cool-down, the chamber pressure never fell below 3×10^{-9} torr. This was considered unacceptable for installing the trap. Subsequent vacuum tests of chamber components showed persistent contamination of the trap chamber by PEEK residue. This contamination could not be removed even by baking the all-metal components of the chamber at 350 C for over a week.

We attribute the contamination to imperfect temperature control during the bake. For our baking apparatus, the difference between the measured temperature and the temperature at the socket could easily reach 10 – 20 C, while the superior GTRI facilities would probably hold this difference below 5 C. While we were unable to find any systematic outgassing studies of PEEK in the literature, the continuous use temperature for PEEK in air is given as 260 C by most manufacturers. Moreover, PEEK exhibits substantial changes to its mechanical properties when heated to 275 C under high vacuum [Murari04]. It is easy to imagine that we exceeded the critical temperature for PEEK decomposition and outgassing.

To achieve good vacuum, we performed a thorough ultrasonic cleaning of the Kimball Physics chamber, socket, and feedthroughs, and re-baked this section at 200 C for 15 days. At that point, no PEEK contamination could be observed at the RGA – only a residue of methane, with partial pressure of a few parts in 10^{-10} torr. We completely rebuilt the remainder of the chamber from all-new components and baked this section separately at 250 C for 20 days. We then combined the two sections, inserted the Microwave I trap, and baked at 150 C for 5 days. We obtained a final pressure of 3×10^{-11} torr as measured by the ion gauge. Note that these gauge measurements are systematically higher than GTRI pressure measurements derived from the ion pump current, so our measured pressure is roughly the same as that measured by GTRI.

We recommend that PEEK components not be heated past 200 C. It appears that a 200 C bake is quite sufficient to passivate the PEEK outgassing, without the risk of PEEK decomposition and chamber contamination.

Obstacles and solutions for electrical connections

The PEEK socket that holds the trap carrier is a delicate and complex device which requires a number of specialized tools for assembly. The socket at Griffith was manufactured at GTRI using components machined at Griffith. Significant support by GTRI was necessary for successful operation of the socket after delivery. The GTRI team were of tremendous help and we offer these comments purely as suggestions for improvement in future versions.

Several of the wires into the socket broke at the crimp connectors into their individual socket pins. Because these connections are made with solid-core wire, they are relatively fragile. The large number of wires (100 for our socket) and the restricted space in the vacuum chamber makes it difficult to manipulate the wires with the required delicacy. These wires could not be repaired without specialized equipment and training. Replacements were sent from GTRI. It might be possible to strain-relief the wires with an additional plate behind the socket.

Disassembling the socket, as required for replacement of the wires, nearly failed because of galling of the screws. Several of the screws holding down the top socket plate could not be removed. The screw heads stripped and the screw heads had to be ground off using a metal bit. A small amount of the PEEK material of the socket plate was scratched and/or burned in this process. Fortunately, the pressure obtained after bake shows that the damaged material had a surprisingly low outgassing rate. Future designs might avoid this by using gold-plated screws similar to those used in the rest of the socket.

The coaxial cables for in-vacuum microwave connections are quite inflexible, as expected for any cable carrying 12.6 GHz signal. Thermal relaxation of the cables during the bake actually forced the trap carrier up and out of the socket on two occasions. We installed a cable guide (simply a metal plate with a ½" hole, located near the trap carrier) that effectively prevented the cables from moving transversely to the trap microwave connectors. The issue appears solved.

3.2.2 Laser systems

Sub-Doppler spectroscopy

We have implemented an improved laser locking system for our 370 nm laser based on Yb^+ ions in a discharge lamp. The setup is essentially that of polarization spectroscopy [Polspec], but with a chopped pump beam to improve noise rejection. This system provides sub-Doppler locking features at all isotope peaks. The locking system is now routinely used for laser cooling of Yb^+ to the Doppler limit in our needle trap. This work was performed in collaboration with Dr. Michael Biercuk of the University of Sydney.

The limiting factor in the linewidth of the locking features appears to be residual Doppler shift. These arise from the laser geometry – within our space constraints, it is difficult to obtain perfectly counterpropagating pump and probe beams. Under optimized conditions, we have observed signal linewidths as small as 100 MHz, better than any currently reported for ions in a discharge lamp.

370 nm external-cavity diode laser

Maintaining the 370 nm laser system for laser cooling of Yb^+ presented some difficulty during this project. A number of recently procured Nichia diode lasers exhibited sharply reduced lifetimes as compared to previous lasers, with UV damage to the laser window occurring on the order of weeks or months compared to the ~1 year lifetime of previous lasers.

Nichia no longer manufactures the 20 mW, 375 nm laser diodes that are used in 370 nm Yb^+ cooling lasers around the world. Instead, they manufacture a new 70 mW, 375 nm model. We tested this model in our external cavity system and found that it was substantially less stable. In particular, the mode structure seems very delicate and near-perfect reimaging of the mode is necessary for good feedback.

Our home-built external cavity laser has been replaced by a commercial Moglabs model which has better optomechanical flexibility and stability. The system uptime is substantially improved and we recommend the Moglabs system to other researchers.

4 Characterization

4.1 *GTRI Operation*

The first IDM trap to be packaged (a hybrid optic chip) was damaged during packaging. An impact to the surface caused shorting of several control electrodes to ground, but not damaging the diffractive optics. Since these shorts would complicate transport of ions over the region just past the load zone, a second IDM chip (also Hybrid) was packaged for delivery to Griffiths. GTRI installed the first trap in the GTRI testing system in order to demonstrate the basic operation of the device. The IDM trap is electrically the same as the GTRI microwave traps, permitting the use of the same basis set of trapping potentials as the microwave trap except for the region around the shorted electrodes. We recalculated the waveforms around these electrodes to compensate for the shorts using the electrostatic model for the original microwave trap.

We installed the IDM trap into a standard GTRI chamber with 100-pin socket. The particular load zone design used in this trap requires voltages beyond the ±10 V provided by our DAC system. We used an amplifier system to increase the voltage range to ±20 V. The ions loaded quickly and we were able to transport out of the load zone as expected.

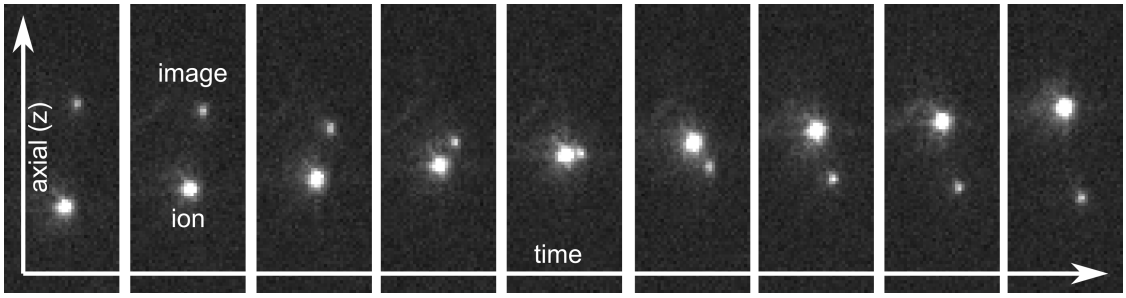

Figure 19: Ion transport over the imaging optic.

We investigated several of the optics and did rough characterization of two of them: a self-focusing optic and a collimating optic. The characterization of the self-focusing optic was fairly straight forward, with images of the ion and its imaged focus taken as the ion was slowly transported axially across the diffractive optic (Figure 19). The reflected image is radially displaced from the ion due to an approximately 1 um radial displacement of the IDM optic from the trap axis. As a test, we pushed the ion radially, off the RF null, and showed that we could

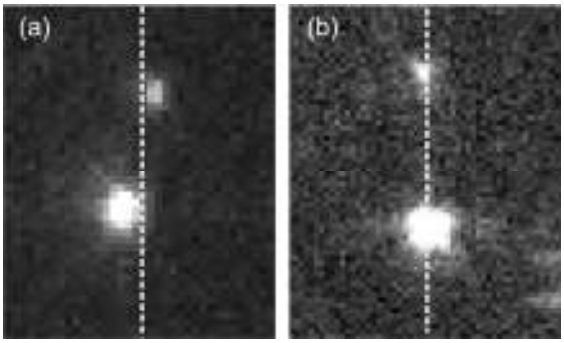

Figure 20: (a) Ion and image alignment when micromotion nulled. (b) Applied radial electric field pushes the ion to the right, with a corresponding movement of the image to the left.

align the two images (Figure 20). Because of the nonlinear EM gain in this EMCCD, the relative brightness of the image cannot be used to estimate the reflectivity of the optic.

The reflective objective used in this testing has an annular front aperture, with the center blocked by the second mirror of the objective as shown in Figure 21. The second mirror of the objective would occlude collimated light in the ideal situation where the IDM optic, ion, and objective lens were all aligned on a common axis. To allow collection of collimated light from the ion through the center of the iris, the ion had to be to one side of the optic (Figure 21). The best alignment was found empirically. With the iris closed to its minimum aperture, the depth-of-field is large enough that the occlusions by the front mirror become roughly in focus as shown in Figure 22.

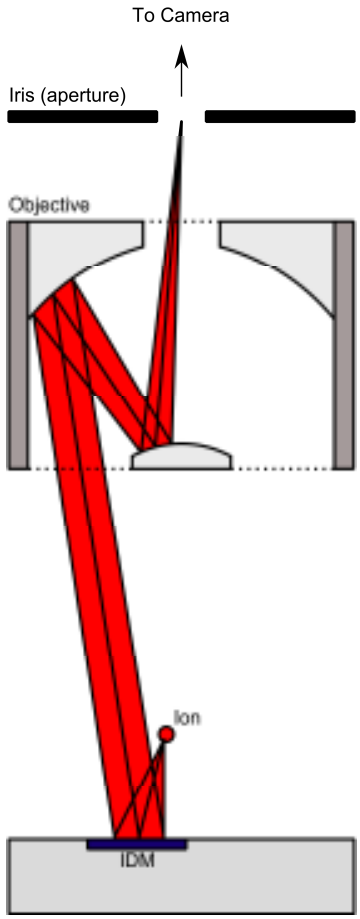

Figure 21: Rough diagram of light collection from IDM with the reflective objective. The collimating optic collection efficiency data were taken so such that the light would both be collected by the lens and pass through the iris when the iris was closed.

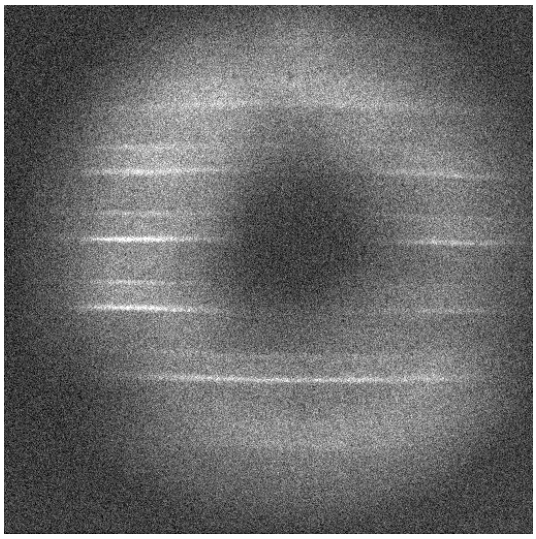

Figure 22: With the lens aperture closed, the depth-of-field is large enough that the central obscuration of the objective is visible as a dark inner region. The bright horizontal bands are patterns on the trap surface.

Figure 23 shows an image of the ion with the iris fully open and another image with the iris at its minimum opening. In the former case, we collect both the direct light from the ion (the bright circle) and the indirect, collimated light, which is difficult to make out over scatter on the trap surface. With the iris closed, we reduce the effective numerical aperture of the lens, blocking the bulk of the direct light and the surface scatter. However, the collimated light is roughly focuses through the iris opening and not affected. To get a better idea of the enhancement from the IDM collimator, we measured the photon collection on the PMT as a function of the ion position across the IDM under both the iris open and iris closed conditions. The resulting photon count vs. ion position plots are shown in Figure

24. In both cases, the fluorescence 397nm laser tracked the ion position to keep a constant laser intensity on the ion. The plots have been corrected for background scatter via measurements taken for both configurations after the ion was lost.

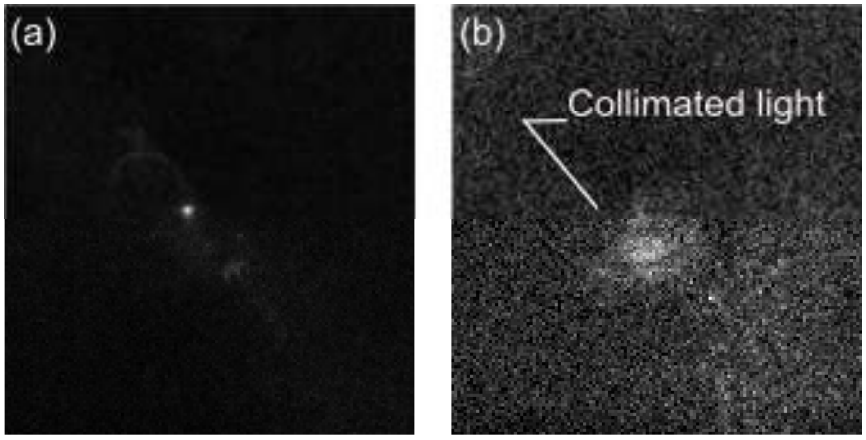

Figure 23: (a) Direct (iris full open) and (b) collimated light (iris closed to minimum) from the ion.

In the aperture (iris) open case, the collection from the direct light is roughly 0.8 photons for a fixed measurement time and is independent of ion position for the range of ion positions shown in the plot. Over a narrow range of ion positions, the collimated light is also collected by the objective, boosting the light collection. As in the previous images, closing the iris effectively reducing the numerical aperture of the lens, suppressing direct light with little or no effect on the collimated light.

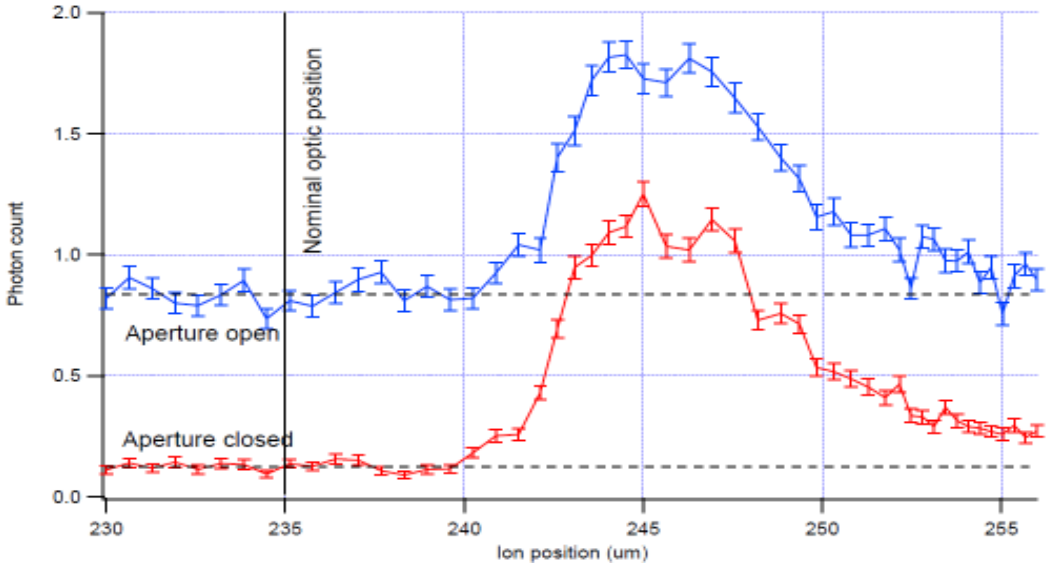

Figure 24: PMT counts vs. ion position over the collimating optic for the lens aperture (iris) fully open and for the aperture at minimum ("closed"). The dashed lines are guides for the eye, showing the photon counts for the direct light from the ion, as extrapolated from the measurements in left wing of the plot. Both measurements have had position dependent backgrounds (measured separately without an ion) subtracted out.

From this plot we can form a rough estimate of the collection efficiency. The NA 0.28 optic produces 0.8 counts while the collimated collection produces 1.0 counts. Assuming no vignetting and approximately isotropic attenuation, the effective geometric NA of the diffractive optic is $0.28\sqrt{1.0/0.8}$ = 0.31, or 2.5% geometric collection efficiency.

4.2 *Griffith Operation*

The Griffith team successfully trapped single ions in the IDM trap using the same RF and DC voltages used for trapping in the Microwave I trap. Evidently, the nanostructuring of the ground electrode surface in the IDM trap does not decrease the RF breakdown voltage much, if at all. An image of an ion in the IDM trap, obtained using a bulk-optics imaging system, is shown in Figure 25. Note this is *not* an image obtained with the diffractive mirror, but bulk-optics imaging serves as a useful starting point.

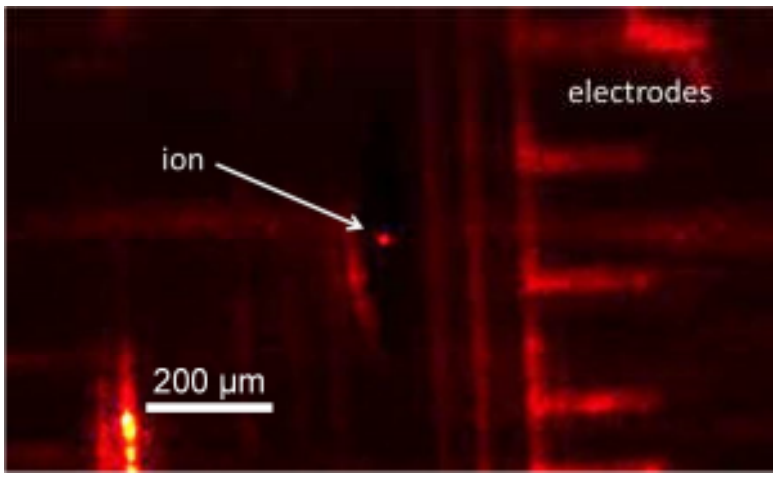

Figure 25. A single ion trapped in the IDM trap loading region. Imaging was performed using the bulk-lens objective. The diffractive mirrors were *not* used to obtain this image.

We have obtained images of ion fluorescence from the diffractive collimation mirror in the loading zone (Figure 26). To estimate the collection efficiency of the diffractive mirror, we imaged the ion using alternately the bulk-lens objective and the diffractive mirror. Integrating the total amount of fluorescence present in each image, we find that the collection efficiencies are equal to within 20%. The numerical aperture of the bulk-lens objective is 0.39, so the nominal collection efficiency of the loading-zone diffractive collimating mirror is estimated as 4 ± 1%. Notably, the loading zone mirror comprises only the edges of the ground electrode around the loading zone – the central portion of the mirror is removed in the laser ablation of the loading hole. The collection efficiency should be substantially higher for the other collimating mirrors, which do not suffer from this defect. Disagreement with the GTRI collection efficiency may indicate that either the GTRI system vignettes the collimated light or the optic efficiency is degraded at 397nm.

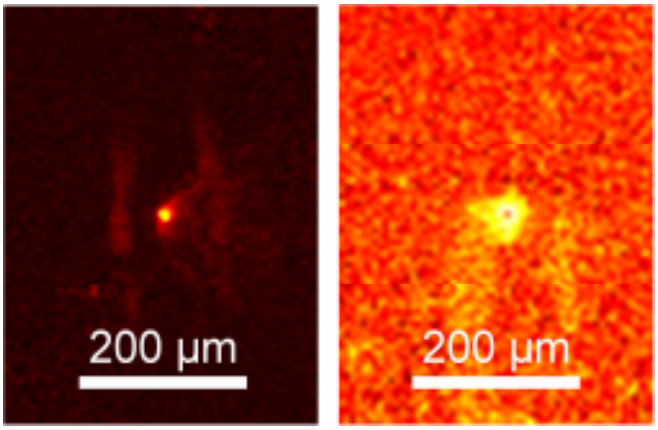

Figure 26. Comparison between bulk-lens and diffractive mirror imaging for a single ion in the IDM trap. Both images are taken under identical camera integration conditions and are background-subtracted to remove scattered light. Left: bulk-lens image. Right: diffractive mirror image obtained with the loading zone collimator. The fluorescence collection efficiency is estimated as 4% (see text).

As in our earlier work with Fresnel lenses, diffraction-limited images will only be obtained when the ion is positioned correctly relative to the diffractive optic. Time constraints prevented us from properly optimizing the imaging. However, we performed a preliminary investigation of the dependence of imaging quality on ion position. Moving the ion along the trap axis by several microns yielded the image shown in Figure 27. Note that this figure still shows a *single* ion, as verified by imaging using the bulk-lens objective. Such "duplicated" images were observed in our earlier work with Fresnel lenses when the imaging aberrations were poorly corrected. Moving the ion by sub-micron distances perpendicular to the trap surface was found to change the spacing between the "duplicate" images, again pointing to aberrations as the cause. At this stage of optimization, aberrations of the bulk-optic objective are also likely to play a significant role in the imaging.

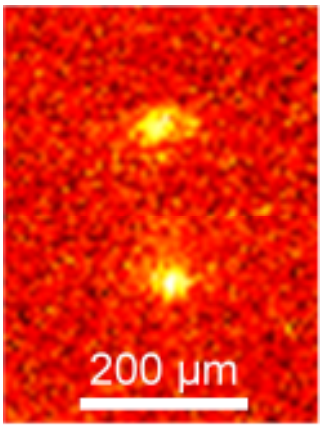

Figure 27. Image of a single ion using the loading-zone diffractive mirror. The image was obtained by moving the ion several microns along the trap axis relative to the image in Figure 26. The apparent "duplication" of the image is consistent with aberrations of the imaging system.

1. T. Shiono, M. Kitagawa, K. Setsune, and T. Mitsuyu, Appl. Opt. 28, 3434 (1989).

2. D. Mikolas, R. Bojko, H. G. Craighead, F. Haas, D. A. Honey, and H. F. Bare, J Vac Sci Technol B 12, 20 (1994).

3. Christopher M. Shappert, J. True Merrill, K. R. Brown, Jason M. Amini, Curtis Volin, S. Charles Doret, Harley Hayden, C-S Pai, Kenneth R. Brown, and Alexa W. Harter, New J. Phys. 15, 083053 (2013).

[4] e.g., Xianzhong Lang, Teng Qiu, Kailin Long, Di Han, Haiyan Nan and Paul K Chu Nanotechnology 24 (2013) 255303

[5] D.Y.R. Chong, W.E. Lee, J.H.L. Pang, T.H. Low, B.K. Lim, Proc Inter Society Conference on Thermal Phenomena, ITherm, Nevada, USA, June 2004, pp. 203-210.

6. Kenneth Wright, Jason M Amini, Daniel L Faircloth, Curtis Volin, S Charles Doret, Harley Hayden, C-S Pai, David W Landgren, Douglas Denison, Tyler Killian, Richart E Slusher, and Alexa W Harter, New J. Phys. 15, 033004 (2013).

7. S. Charles Doret, Jason M. Amini, Kenneth Wright, Curtis Volin, Tyler Killian, Arkadas Ozakin, Douglas Denison, Harley Hayden, C.-S. Pai, Richart E. Slusher, Alexa W. Harter, New J. Phys. **14**, 073012 (2012).

REPORT A

Integrated Diffractive Mirrors for Trapped-Ion Information Processing

Reporting Period: ***(DecFY14)***

Submitted To: IARPA Contracting Agent Workarea at https://www.intelink.gov/sites/iarpa_caw or emailed to PM and Programmatic SETA

ORGANIZATION NAME:	**Georgia Tech Applied Research Corporation**		
Contract Number:	W911NF-12-1-0600		
Task Order Number:			
Name of Effort/Task Name:	Integrated Diffractive Mirrors for Trapped-Ion Information Processing		
Period of Performance:	10/1/2012	through	9/30/2013
Contracting Officer:	Dr. T.R.Govindan		
COTR:			
Principal Investigator:	Dr. Curtis Volin, (404) 407-8487, curtis.volin@gtri.gatech.edu		
Report prepared by:	Curtis Volin		
Phone:	404 407 8487		
Email:	curtis.volin@gtri.gatech.edu		
Address:	400 10th St NW		

Milestones	Status	Due Date
Completed substrate to Fraunhofer	Complete	1-Jan-13
Completed ion trap with diffractive mirror	Complete	1-Sep-13

1.0 Accomplishments/Deliverables - See Attached MSWord Document

2.0 Planned Activities - See Attached MSWord Document

3.0 Issues/Concerns - (New, Open, Resolved) - See Attached MSWord Document

4.0 Financials

In-Progress
On-Time
Late
Complete

Contract/Task Order Award Date	Funded amount	Total Funded Amount	Reason for MOD
Base Contract/Sep 28, 2012	$862,802.00	$862,802.00	
TOTAL	**$862,802.00**	$ 862,802.00	

4.1 Invoices

Invoice Number	Amount Invoiced	Invoice Date	Invoice Paid Date
Invoice Number 1	$ 23,184.29	10/28/2012	
Invoice Number 2	$ 21,614.72	11/28/2012	
Invoice Number 3	$ 57,077.35	12/2012	
Invoice Number 4	$ 58,041.90	1/2013	
Invoice Number 5	$ 33,577.66	2/2013	
Invoice Number 6	$ 131,261.19	3/1/2013	
Invoice Number 7			
Invoice Number 8	$ -		
Invoice Number 9	$ -		
Invoice Number 10	$ -		
Invoice Number 11	$ -		
Invoice Number 12	$ -		
TOTAL	$324,757.11		

4.2 CLIN Summary

Project Name	Funded	Expended	Remaining	Percent Expended
Labor	$ 349,387.99	$ 338,400.75	$ 10,987.24	96.9%
Travel	$ -	$ -	$ -	0.0%
ODCs	$ 513,414.01	$ 523,786.25	$ (10,372.24)	102.0%
Total	$ 862,802.00	$ 862,187.00	$ 615.00	99.9%

4.3 Expenditures - Totals **-7%** **Variance**

Name of Effort	Planned - Total	Planned (Cum)	Actual Incurred - Total	Actual Incurred (Cum)	Monthly Planned v. Actual Variance	Cumulative Planned v. Actual Variance	Variance % (Month)	Estimate at Completion	Cumulative Remaining Funding	% Expended	Funded Value	Funded (Cum)	Invoiced	Invoiced (Cum)
Oct-12	$ 59,750.00	$ 59,750.00	$ 23,184.29	$ 23,184.29	$ (36,565.71)	$ (36,565.71)	-61.20%	$ 826,236.29	$ 839,617.71	2.69%	$ 862,802.00	$ 862,802.00	$ 23,184.29	23184.29
Nov-12	$ 74,500.00	$ 134,250.00	$ 21,614.72	$ 44,799.01	$ (52,885.28)	$ (89,450.99)	-70.99%	$ 773,351.01	$ 818,002.99	5.19%		$ 862,802.00	$ 21,614.72	44799.01
Dec-12	$ 74,000.00	$ 208,250.00	$ 57,077.35	$ 101,876.36	$ (16,922.65)	$ (106,373.64)	-22.87%	$ 756,428.36	$ 760,925.64	11.81%		$ 862,802.00	$ 57,077.35	101876.4
Jan-13	$ 73,500.00	$ 281,750.00	$ 58,041.90	$ 159,918.26	$ (15,458.10)	$ (121,831.74)	-21.03%	$ 740,970.26	$ 702,883.74	18.53%		$ 862,802.00	$ 58,041.90	159918.3
Feb-13	$ 73,000.00	$ 354,750.00	$ 33,577.66	$ 193,495.92	$ (39,422.34)	$ (161,254.08)	-54.00%	$ 701,547.92	$ 669,306.08	22.43%		$ 862,802.00	$ 33,577.66	193495.9
Mar-13	$ 71,939.00	$ 426,689.00	$ 131,261.19	$ 324,757.11	$ 59,322.19	$ (101,931.89)	82.46%	$ 760,870.11	$ 538,044.89	37.64%		$ 862,802.00	$ 131,261.19	324757.1
Apr-13	$ 70,500.00	$ 497,189.00	$ 122,681.78	$ 447,438.89	$ 52,181.78	$ (49,750.11)	74.02%	$ 813,051.89	$ 415,363.11	51.86%		$ 862,802.00	$ -	324757.1
May-13	$ 70,500.00	$ 567,689.00	$ 57,198.92	$ 504,637.81	$ (13,301.08)	$ (63,051.19)	-18.87%	$ 799,750.81	$ 358,164.19	58.49%		$ 862,802.00	$ -	324757.1
Jun-13	$ 70,500.00	$ 638,189.00	$ 88,196.12	$ 592,833.93	$ 17,696.12	$ (45,355.07)	25.10%	$ 817,446.93	$ 269,968.07	68.71%		$ 862,802.00	$ -	324757.1
Jul-13	$ 83,485.00	$ 721,674.00	$ 80,778.18	$ 673,612.11	$ (2,706.82)	$ (48,061.89)	-3.24%	$ 814,740.11	$ 189,189.89	78.07%		$ 862,802.00	$ -	324757.1
Aug-13	$ 70,500.00	$ 792,174.00	$ 89,713.27	$ 763,325.38	$ 19,213.27	$ (28,848.62)	27.25%	$ 833,953.38	$ 99,476.62	88.47%		$ 862,802.00		324757.1
Sep-13	$ 70,628.00	$ 862,802.00	$ 98,861.62	$ 862,187.00	$ 28,233.62	$ (615.00)	39.98%	$ 862,187.00	$ 615.00	99.93%		$ 862,802.00		324757.1
TOTAL	**$ 862,802.00**	**$ 862,802.00**	**$ 862,187.00**	**$ 862,187.00**	**$ (615.00)**	**$ (615.00)**	**-66.09%**	**$ 862,187.00**	**$ 615.00**	**99.93%**	**$ 862,802.00**	**$ 862,802.00**	**324757.11**	**324757.1**

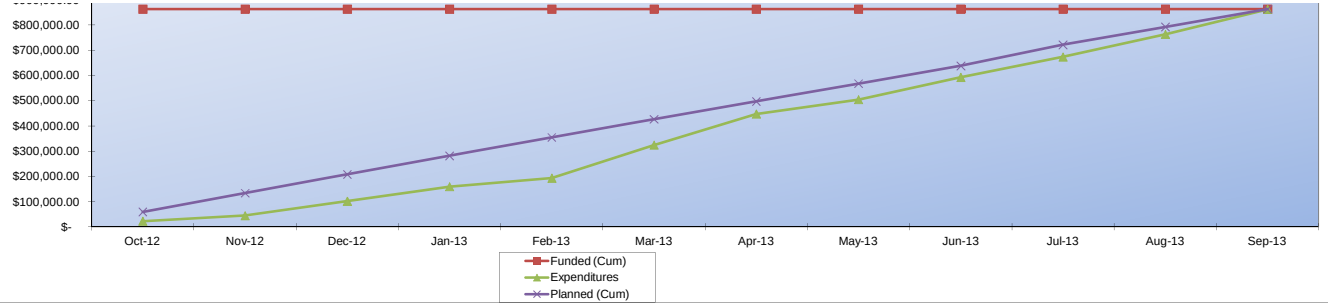

Explain Variance of Planned versus Actuals

4.4 Expenditures - Labor

Name of Effort	Planned Expended - Labor	Planned Expended (Cum)	Actual Expended - Labor	Actual Expended (Cum)	Monthly Planned v. Actual Variance	Cumulative Planned v. Actual Variance	Variance % (Month)	Estimate at Completion	Cumulative Remaining Funding	% Expended
Oct-12	$15,000.00	$ 15,000.00	$ 15,853.80	$ 15,853.80	$ 853.80	$ 853.80	5.69%	$ 350,241.79	$ 333,534.19	4.54%
Nov-12	$30,400.00	$ 45,400.00	$ 20,946.88	$ 36,800.68	$ (9,453.12)	$ (8,599.32)	-31.10%	$ 340,788.67	$ 312,587.31	10.53%
Dec-12	$30,400.00	$ 75,800.00	$ 18,430.71	$ 55,231.39	$ (11,969.29)	$ (20,568.61)	-39.37%	$ 328,819.38	$ 294,156.60	15.81%
Jan-13	$30,400.00	$ 106,200.00	$ 33,442.22	$ 88,673.61	$ 3,042.22	$ (17,526.39)	10.01%	$ 331,861.60	$ 260,714.38	25.38%
Feb-13	$30,400.00	$ 136,600.00	$ 31,813.74	$ 120,487.35	$ 1,413.74	$ (16,112.65)	4.65%	$ 333,275.34	$ 228,900.64	34.49%
Mar-13	$30,400.00	$ 167,000.00	$ 19,100.11	$ 139,587.46	$ (11,299.89)	$ (27,412.54)	-37.17%	$ 321,975.45	$ 209,800.53	39.95%
Apr-13	$30,400.00	$ 197,400.00	$ 13,596.14	$ 153,183.60	$ (16,803.86)	$ (44,216.40)	-55.28%	$ 305,171.59	$ 196,204.39	43.84%
May-13	$30,400.00	$ 227,800.00	$ 25,296.15	$ 178,479.75	$ (5,103.85)	$ (49,320.25)	-16.79%	$ 300,067.74	$ 170,908.24	51.08%
Jun-13	$30,400.00	$ 258,200.00	$ 54,380.41	$ 232,860.16	$ 23,980.41	$ (25,339.84)	78.88%	$ 324,048.15	$ 116,527.83	66.65%
Jul-13	$30,400.00	$ 288,600.00	$ 27,248.21	$ 260,108.37	$ (3,151.79)	$ (28,491.63)	-10.37%	$ 320,896.36	$ 89,279.62	74.45%
Aug-13	$30,400.00	$ 319,000.00	$ 44,025.10	$ 304,133.47	$ 13,625.10	$ (14,866.53)	44.82%	$ 334,521.46	$ 45,254.52	87.05%
Sep-13	$30,387.99	$ 349,387.99	$ 34,267.28	$ 338,400.75	$ 3,879.29	$ (10,987.24)	12.77%	$ 338,400.75	$ 10,987.24	96.86%
TOTAL	**$ 349,387.99**	**$ 349,387.99**	**$ 338,400.75**	**$ 338,400.75**	**$ (10,987.24)**	**$ (10,987.24)**	**-12.70%**	**$ 338,400.75**	**$ 10,987.24**	**96.86%**

4.5 Expenditures - Trave

Name of Effort	Planned Expended - Travel	Planned Expended (Cum)	Actual Expended - Travel	Actual Expended (Cum)	Monthly Planned v. Actual Variance	Cumulative Planned v. Actual Variance	Variance % (Month)	Estimate at Completion	Cumulative Remaining Funding	% Expended
Oct-12	$ -	$ -	$ -	$ -	$ -	$ -	0.00%	$ -	$ -	0.00%
Nov-12	$ -	$ -	$ -	$ -	$ -	$ -	0.00%	$ -	$ -	0.00%
Dec-12	$ -	$ -	$ -	$ -	$ -	$ -	0.00%	$ -	$ -	0.00%
Jan-13	$ -	$ -	$ -	$ -	$ -	$ -	0.00%	$ -	$ -	0.00%
Feb-13	$ -	$ -	$ -	$ -	$ -	$ -	0.00%	$ -	$ -	0.00%
Mar-13	$ -	$ -	$ -	$ -	$ -	$ -	0.00%	$ -	$ -	0.00%
Apr-13	$ -	$ -	$ -	$ -	$ -	$ -	0.00%	$ -	$ -	0.00%
May-13	$ -	$ -	$ -	$ -	$ -	$ -	0.00%	$ -	$ -	0.00%
Jun-13	$ -	$ -	$ -	$ -	$ -	$ -	0.00%	$ -	$ -	0.00%
Jul-13	$ -	$ -		$ -	$ -	$ -	0.00%	$ -	$ -	0.00%
Aug-13	$ -	$ -		$ -	$ -	$ -	0.00%	$ -	$ -	0.00%
Sep-13	$ -	$ -		$ -	$ -	$ -	0.00%	$ -	$ -	0.00%
TOTAL	**$ -**	**$ -**	**$ -**	**$ -**	**$ -**	**$ -**	**0.00%**	**$ -**	**$ -**	**0.00%**

4.6 Expenditures - ODCs

Name of Effort	Planned Expended - ODCs	Planned Expended (Cum)	Actual Expended - ODCs	Actual Expended (Cum)	Monthly Planned v. Actual Variance	Cumulative Planned v. Actual Variance	Variance % (Month)	Estimate at Completion	Cumulative Remaining Funding	% Expended
Oct-12	$44,750.00	$ 44,750.00	$ 7,330.49	$ 7,330.49	$ (37,419.51)	$ (37,419.51)	-83.62%	$ 475,994.50	$ 506,083.52	1.43%
Nov-12	$44,100.00	$ 88,850.00	$ 667.84	$ 7,998.33	$ (43,432.16)	$ (80,851.67)	-98.49%	$ 432,562.34	$ 505,415.68	1.56%
Dec-12	$43,600.00	$ 132,450.00	$ 38,646.64	$ 46,644.97	$ (4,953.36)	$ (85,805.03)	-11.36%	$ 427,608.98	$ 466,769.04	9.09%
Jan-13	$43,100.00	$ 175,550.00	$ 24,599.68	$ 71,244.65	$ (18,500.32)	$ (104,305.35)	-42.92%	$ 409,108.66	$ 442,169.36	13.88%
Feb-13	$42,600.00	$ 218,150.00	$ 1,763.92	$ 73,008.57	$ (40,836.08)	$ (145,141.43)	-95.86%	$ 368,272.58	$ 440,405.44	14.22%
Mar-13	$41,539.00	$ 259,689.00	$ 112,161.08	$ 185,169.65	$ 70,622.08	$ (74,519.35)	170.01%	$ 438,894.66	$ 328,244.36	36.07%
Apr-13	$40,100.00	$ 299,789.00	$ 109,085.64	$ 294,255.29	$ 68,985.64	$ (5,533.71)	172.03%	$ 507,880.30	$ 219,158.72	57.31%
May-13	$40,100.00	$ 339,889.00	$ 31,902.77	$ 326,158.06	$ (8,197.23)	$ (13,730.94)	-20.44%	$ 499,683.07	$ 187,255.95	63.53%
Jun-13	$40,100.00	$ 379,989.00	$ 33,815.71	$ 359,973.77	$ (6,284.29)	$ (20,015.23)	-15.67%	$ 493,398.78	$ 153,440.24	70.11%
Jul-13	$53,085.00	$ 433,074.00	$ 53,529.97	$ 413,503.74	$ 444.97	$ (19,570.26)	0.84%	$ 493,843.75	$ 99,910.27	80.54%
Aug-13	$40,100.00	$ 473,174.00	$ 45,688.17	$ 459,191.91	$ 5,588.17	$ (13,982.09)	13.94%	$ 499,431.92	$ 54,222.10	89.44%
Sep-13	$40,240.01	$ 513,414.01	$ 64,594.34	$ 523,786.25	$ 24,354.33	$ 10,372.24	60.52%	$ 523,786.25	$ (10,372.24)	102.02%
TOTAL	**$ 513,414.01**	**$ 513,414.01**	**$ 523,786.25**	**$ 523,786.25**	**$ 10,372.24**	**$ 10,372.24**	**-91.05%**	**$ 523,786.25**	**$ (10,372.24)**	**102.02%**

Description of Equipment Purchased	Model Number	Serial Number	Unit Cost of Equipment	Number of Units	Total Cost	Date of Purchase	Location of Equipment	Method Obtained	Reason for Purchase

5.0 Inventory of Government Property Procured-If no property was procured in any given month please add a note saying that
Government Auditable Property (Equipment > $50,000) Invoices must be submitted monthly

Description of Equipment Purchased	Model Number	Serial Number	Unit Cost of Equipment	Number of Units	Total Cost	Planned Purchase Date	Date of Purchas	Location of Equipment	Reason for Purchase
No property to date									

Government Accountable Property (Equipment $5,000 < $49,999)

		Task Order Number	Equipment Description	Location	ria	Bar Code	Date Acquired	Unit Price	rvice Date	Amount Invoiced	Receipt #	